Asian Journal of Chemistry; Vol. 29, No. 12 (2017), 2692-2700

ASIAN JOURNAL OF CHEMISTRY

https://doi.org/10.14233/ajchem.2017.20806

Improvement of Indoor Air Quality by Applying $LiNbO_3$ on Concrete

RANJIT K. NATH[1,2,*], M.K. MOHAMMAD ZIAUL HYDER[1,*] and M.F.M. ZAIN[2]

[1]Department of Chemistry, Faculty of Engineering & Technology, Chittagong University of Engineering and Technology (CUET), Chittagong-4349, Bangladesh

[2]Sustainable Construction Materials and Building Systems Research Group, Faculty of Engineering and Built Environment, Universiti Kebangsaan Malaysia, 43600 UKM Bangi, Malaysia

*Corresponding authors: E-mail: rkn_chem@yahoo.com; ziaulhyder@cuet.ac.bd

Received: 23 May 2017; *Accepted*: 17 July 2017; *Published online*: 30 October 2017; AJC-18617

Photocatalysts in ordinary building materials such as concrete create environment-friendly materials by which air pollution can be diminished. In this study, $LiNbO_3$-coated concrete block was used to investigate pollutant removal efficiency, wherein toluene and ethylbenzene were selected as common indoor air pollutants. The effectiveness of using immobilized $LiNbO_3$ to remove ethylbenzene and toluene from indoor air was investigated under various operational parameters. About 80 % of toluene and 82.5 % of ethylbenzene could be removed within 6 h under ultraviolet-visible light illumination using $LiNbO_3$ as a photocatalyst in concrete. Therefore, in the near future, $LiNbO_3$ may be used as a sustainable construction material that could contribute to indoor air purification

Keywords: Indoor air quality, $LiNbO_3$, Photocatalytic degradation, Volatile organic compounds.

INTRODUCTION

People generally spend the majority of their time in indoor environments. Indoor environmental quality is a key aspect in the evaluation of meeting the concept of green building aimed at sustainable development for non-residential buildings, such as commercial, institutional, and industrial ones. Therefore, indoor air quality directly affects human health in terms of lengthened exposure to pollutants by inhalation [1,2] and volatile organic compounds (VOCs) play an important role in polluting indoor environments. Volatile organic compounds (VOCs) are compounds containing at least one carbon and a hydrogen atom in its molecular structure and have a boiling point between 50 and 260 ºC [3]. A great variety of organic materials have been identified in indoor air. These materials include aliphatic and aromatic hydrocarbons, chlorinated hydrocarbons and various ketones and aldehydes [4]. Many VOCs are toxic and some are even considered mutagenic, teratogenic [5,6] or carcinogenic (*e.g.*, benzene, ethylbenzene, and toluene). Nevertheless, the actual health implications of most of the organic compounds found in indoor air are not presently well defined. Exposure to VOCs can result in both acute and chronic health problems. Asthmatics and other individuals with prior respiratory complaints may be particularly susceptible to low-dose VOC exposures [7-9]. At high concentrations, many VOCs are strong narcotics and can depress the central nervous system [10,11]. Exposures can also lead to the irritation of eyes and respiratory tract and to sensitization reactions involving the eyes, skin and lungs. The occurrence of these compounds in the atmosphere therefore poses a great threat to human health and the environment. Many air-purification methods are available in the literature. Existing technologies such as incineration, absorption, adsorption, and condensation ionization for controlling emissions and improving air quality are not very satisfactory because they degrade air quality [12,13]. Although filtration is the most widely used method because of its low cost and high pollutant removal effectiveness, older air filters have been associated with health issues, increased pollutant concentration and reduced work performance. Systems that are passive, cost effective and work along with existing air handling systems to reduce loading and increase overall energy efficiency are always necessary to develop [14]. One such area that has been widely explored is the use of materials that can be embedded or coated on walls and wall boards that can passively and effectively destroy indoor concentrations of pollutants [15]. Photocatalysis is a very exciting topic in the innovation of the cement industry with sustainable solutions. These innovative products have been developed to provide an environment-friendly solution in the construction industry and are becoming widely recognized for green constructions [16]. A broad utilization of white photocatalytic materials in concrete could enable the reduction of environmental pollution, thereby improving air quality.

Presently, the majority of work in this field involves the use of TiO_2 [1,9]. This material has a bandgap energy of 3.2 eV and thus absorbs in the near ultraviolet (UV) light (about 380 nm). In 2011, Stock and Dunn [11] found that $LiNbO_3$ generated more products under UV and visible irradiation than TiO_2 despite its wider bandgap (3.78 eV). The surprisingly high yield product using $LiNbO_3$ is explained by its strong remnant polarization (70 $\mu C/cm^2$), which is not found in TiO_2. In the present research, experimental results of the photocatalytic removal of ethyl benzene and toluene from indoor environment were discussed. In photodegradation, a catalyst accelerates photoreaction by interacting with substrate in its ground or excited state [17]. In heterogeneous photocatalysis, two active phases, solid and liquid gas, are present [18]. The solid phase is a catalyst, usually a semiconductor [19]. The molecular orbital of semiconductors has a band structure [17]. Bands are distributions of many molecular orbital energy levels, which are so closely spaced in energy that they seem to be continuous. The bands of interest in photocatalysis are populated valence band and its largely vacant conduction band, which is characterized by bandgap energy (E_{bg}) [20,21]. Semiconductors may be photo-excited to form electron-acceptor sites (oxidizing sites) and electron-donor sites (reducing sites), thereby providing great scope for redox reaction [22]. As illustrated in Fig. 1, an electron is promoted from valence band to conduction band, leaving a positive hole in valence band and an electron in conduction band when the semi-conductor is illuminated with light (hν) of greater energy than that of bandgap.

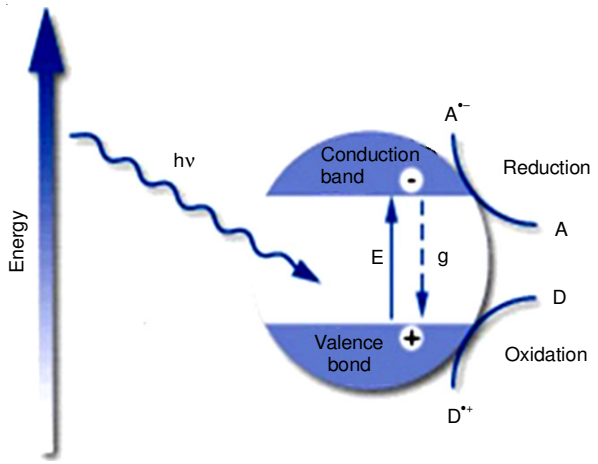

Fig. 1. Mechanism of electron-hole pair formation in a $LiNbO_3$ particle in the presence of pollutant under UV illumination

If charge separation is maintained, electron and hole may migrate to the catalyst surface where they participate in redox reactions with sorbed species. Particularly, the positive hole in valence band (h^+_{vb}) may react with surface-bound H_2O or OH^- to produce hydroxyl radical, and free electron in conduction band (e^-_{cb}) is picked up by oxygen to generate super-oxide radical anion ($O_2^{\bullet-}$) [19,23,24], as indicated in the following eqns 1-3:

The absorption of efficient photons by $LiNbO_3$ ($h\nu \geq E_{bg}$ = 3.78 eV) is

$$LiNbO_3 + h\nu \longrightarrow e^-_{cb} + h^+_{vb} \quad (1)$$

The formation of superoxide radical anion is

$$O_2 + e^-_{cb} \longrightarrow O_2^{\bullet-} \quad (2)$$

The neutralization of OH^- group into $^{\bullet}OH$ by the hole

$$(H_2O \Leftrightarrow H^+ + OH^-)_{ads} + h^+_{vb} \rightarrow {}^{\bullet}OH + H^+ \quad (3)$$

Hydroxyl radical ($^{\bullet}OH$) and superoxide radical anions ($O_2^{\bullet-}$) are the primary oxidizing species in photocatalytic oxidation [25,26]. These oxidative reactions result in the degradation of pollutants as shown in the following eqns. (4 and 5):

The oxidation of organic pollutants through successive attack by ($^{\bullet}OH$) radicals is

$$R + {}^{\bullet}OH \longrightarrow R'^{\bullet} + H_2O \quad (4)$$

or by direct reaction with holes.

$$R + h^+ \longrightarrow R^{\bullet+} \longrightarrow \text{Degradation products} \quad (5)$$

The chain reactions continue until the VOC is completely mineralized to CO_2 and H_2O. Some side reactions may also be induced to generate volatile compounds, thereby accelerating oxidation. For oxidation to occur, the valance band must have a higher oxidation potential than the material under consideration [27]. The redox potential of valance band and conduction band for different semiconductors varies between +4.0 and -3.5 V *versus* standard hydrogen electrode, respectively [28]. Valence band and conduction band energies of $LiNbO_3$ are estimated to be + 0.48 and - 3.30 V, respectively, which means that its bandgap energy is 3.78 eV and thus absorbs in the near-UV light ($\lambda < 339$ nm) [21,29,30]. Most of the VOCs have a higher potential than that of $LiNbO_3$ valance band and can thus be oxidized [31].

EXPERIMENTAL

Ordinary Portland cement, sand and stone aggregates that are commercially available in Malaysia were used to prepare the concrete sample block. Locally available coarse river sand and stone aggregates 8-10 mm in size were used. The specific gravities of sand and aggregates used were 2.63 and 2.65, respectively. $LiNbO_3$ powder CAS12031-63-9 from Sigma-Aldrich was used as photocatalyst. Ethyl benzene and toluene from Sigma-Aldrich were used as pollutants in indoor environment.

The central part of the experimental setup used was a reaction chamber, which allowed a sample size of 10 × 20 cm^2 to be fixed. The reaction chamber was composed of materials that are non-absorbent to the applied pollutants and can hold up UV light with high irradiance. All structural parts inside the box facilitated laminar flow of the gas along sample surface and guaranteed the uniform distribution of the pollutants. A fluorescent lamp with 366 nm wavelength was used to supply photo-irradiation to activate the photocatalyst. Two types of sensors were used to control the temperature and humidity. Fig. 2 shows the illustration of the reaction chamber and the test setup for ethyl benzene and toluene degradation.

Sample preparation: Concrete samples were fabricated in steel molds with internal dimensions of 20 cm × 10 cm × 5 cm. Cement, sand and stone aggregates were thoroughly mixed (mixture ratio = 1:2:4; water-cement ratio = 0.5) and were then poured into the steel mold. Thereafter, compaction was performed by placing the steel molds on a mechanical vibrating table. The top surface of concrete was smoothened with a glass plate. The concrete samples were removed from the molds after 24 h and submerged into water for 28 days for proper curing.

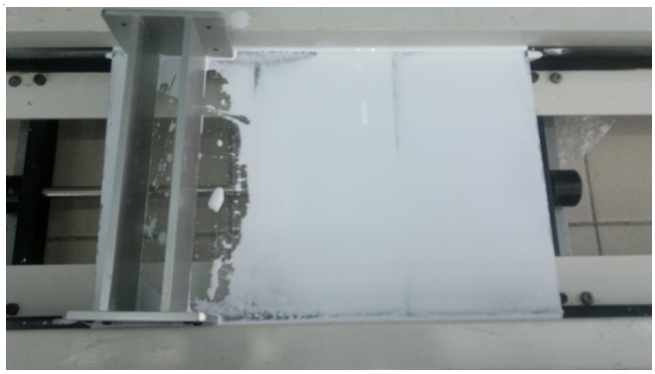

Fig. 2. $LiNbO_3$ coating in glass plate

After curing, samples were allowed to dry in air for few hours. The dried samples were then coated with 0.75 mm $LiNbO_3$ paste. To measure the proper coating thickness for removing maximum VOC, a glass plate was coated with $LiNbO_3$ of various thicknesses [*i.e.*, 0.25, 0.50, and 0.75 mm (Fig. 3)].

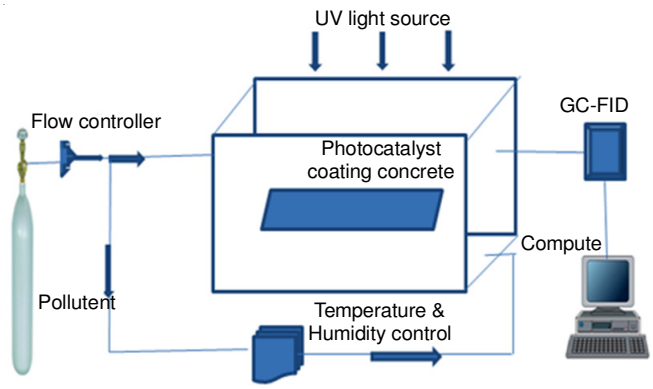

Fig. 3. Schematic diagram of the experimental setup

Experimental procedure and photocatalytic degradation kinetics: The photoreactor was first vacuumed before injecting a quantified gas sample. After preparing the samples and placing them in the reactor, target pollutants (ethyl benzene and toluene) were injected until the concentration reached that when UV illumination was started. The total illumination time of photodegradation was 6 h. Different concentrations of ethyl benzene were individually degraded. To investigate the effect of contact time and pollutant concentration at predetermined time intervals, 5 mL of gas was withdrawn from the reaction chamber and ethylbenzene concentration was measured by gas chromatography with flame ionization detection. The experiment was carried out at room temperature of 25-27 ºC and relative humidity of 50-55 %.

Degradation rate of ethylbenzene was calculated using the following eqn.:

$$Q_{pol_x} = \frac{\int([pol]_o - [pol])dt}{A \times T} \quad (6)$$

where Q_{polx} is the amount of pollution removed by the test sample (mg L^{-1} m^{-2} h^{-1}), $[Pol]_o$ is the injected concentration of pollutant (mg/L), [Pol] is the pollutant concentration after adsorption (mg/L), dt is the time of removal operation (min), A is the surface area of concrete block samples (m^2) and T is the duration of photocatalytic process (6 h for all experiments).

The above equation is known as Langmuir-Hinshel-Wood model, which is widely used to describe the kinetics of gas-solid phase reaction in heterogeneous photocatalysis. This model can be applied to analyze the degradation rate of VOC pollutant conversion in photocatalytic concrete blocks.

RESULTS AND DISCUSSION

Effect of $LiNbO_3$ coating thickness: Ethyl benzene and toluene removal efficiencies of photocatalyst-coated concrete depended on coating thickness. Thus, these efficiencies were investigated by varying the coating thicknesses of $LiNbO_3$. On the concrete surface, 0.25, 0.50 and 0.75 mm thicknesses were difficult to accurately measure because the surface is porous. To measure the proper coating thickness for removing the maximum amount of pollutant such as VOC, $LiNbO_3$ is coated onto glass plates at different thicknesses. Initial concentration is maintained at 50 mg/L into the experimental chamber (reactor).

Removal of ethyl benzene: The removal rate of ethyl benzene at different coating thicknesses are shown in Fig. 4, indicating that removal efficiency increases with increased $LiNbO_3$ coating thickness at an initial concentration of 50 mg/L. The removal efficiency of pollutants depends on the number of active molecules on the surface. $LiNbO_3$ in solid surfaces self-assembles through weak non-covalent interactions and direct assembly of molecules through strong chemical bonds. Molecules of directed-assembly layer cannot directly interact with ethyl benzene. These assemblies originate from interfacial non-covalent interactions or surface chemical reactions at molecular scale. The adsorption of each molecule of a self-assembled monolayer formed on a solid surface includes at least three categories of non-covalent forces. They are interactions between two adjacent molecules in a lamella, interactions between adjacent molecules of two neighbouring lamellae and interactions between molecules and solid surface. These interactions determine molecular activity. If the interaction of self-assembled monolayer with ethyl benzene is higher, the molecular activity of $LiNbO_3$ would be higher, which enhances the photocatalytic removal of ethyl benzene. At 0.25 and 0.5 mm coating thicknesses, $LiNbO_3$ molecules are fewer than those at 0.75 and 1.00 mm coating thicknesses. Thus, removal efficiency is also lower. At 0.75 and 1.00 mm coating thicknesses, the same efficiency is observed because of the presence of maxi-

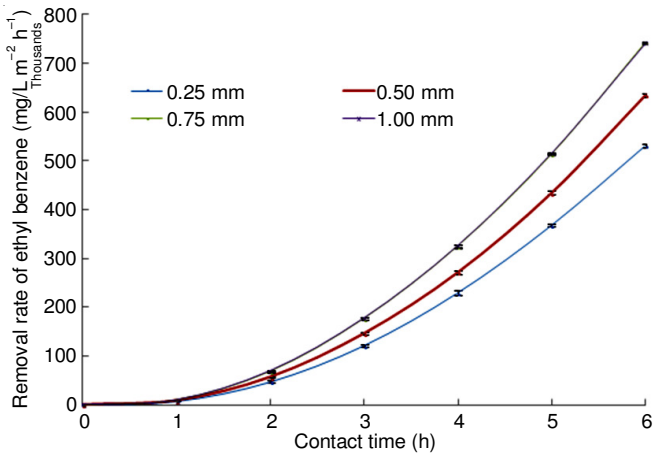

Fig. 4. Removal rate of ethyl benzene from indoor air at different depth of coating at initial concentration 50 mg/L

mum number of active molecules on the surface that are self-assembled. At 1.00 mm coating thickness, the number of $LiNbO_3$ molecules is higher because of the presence of directed-assembly layer that induce some molecules to remain inactive. Similarly, 0.75 and 1.00 mm coating thicknesses yield a similar result.

The percentage degradation of ethyl benzene with respect to contact time of ethyl benzene at different thicknesses of $LiNbO_3$-coated specimens is shown in Fig. 5. The removal percentage of ethyl benzene is higher at the initial stage until 2 h, as illustrated by an initial steeper slope of curve. The initial higher concentration of ethyl benzene explains this steeper slope. After nearly 2 h, the curves become flatter as ethyl benzene concentration decreased with time because of photodegradation. After 1 h, the percentage removals of ethyl benzene for 0.25, 0.50, 0.75, and 1.00 mm coating thicknesses are 29.2, 37.3, 38 and 37.9 %, respectively. Then, after 6 h, the percentages increase to 58.9, 70.5, 82.5 and 82.3 %, respectively. The enhancement of degradation rate is due to the increase in the density of particles in the illumination area. The small height of error bars in terms of standard deviation (Fig. 5) indicates the experimental accuracy.

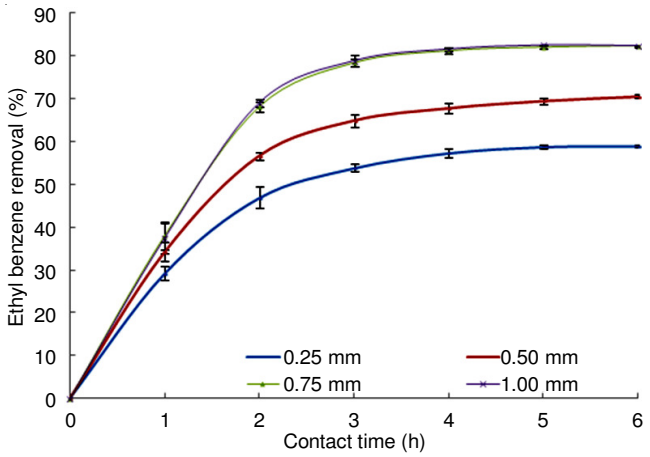

Fig. 5. Effect of depth of coating for the photo degradation of ethyl benzene

Another possible reason is the involvement of charge transfer with $LiNbO_3$ during illumination. Upon illumination, electron-hole pairs are produced on the photocatalyst surface that removed ethyl benzene by degradation. Thus, higher coating thicknesses (0.75 and 1.00 mm) can remove more ethyl benzene by producing more electron-hole pairs than lower coating thicknesses (0.25 and 0.50 mm). Again, at higher coating thicknesses, some photocatalysts are found deeper in the host catalyst, which remains inactive throughout photodegradation. Coatings with 0.75 and 1.00 mm thicknesses yield a similar result.

Removal of toluene: Fig. 6 shows the removal rates of toluene at different coating thicknesses and at an initial toluene concentration of 50 mg/L. Results indicate that decomposition rate gradually increases with increased $LiNbO_3$ coating thickness. This finding is due to the increased number of active (self-assembled) $LiNbO_3$ molecules on the coating surface that interact with toluene under illumination. Afterwards, a certain thickness decomposition rate remains the same because of self- and directed-assembly systems of $LiNbO_3$ molecules. This phenomenon can be attributed to the further absorption of light intensity, which means that catalyst film requires an appropriate number of coats to completely absorb light.

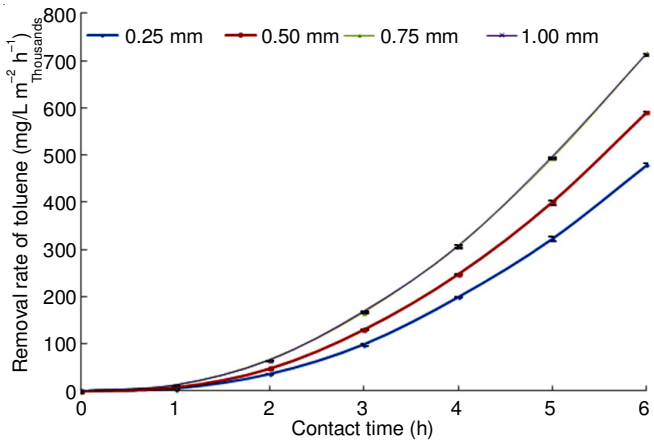

Fig. 6. Removal rate of toluene at different depth of coating

Again, at lower amount of $LiNbO_3$ (*i.e.*, low coating thickness) on the concrete surface, removal rate is lower. This result is expected because the amount of toluene degradation depends on the amount of hydroxyl radicals on the photocatalyst surface, which in turn depends on the number of holes generated on the catalyst surface. Thus, hydroxyl radicals generated at a lower $LiNbO_3$ coating thickness are insufficient to degrade toluene at a high rate, but the amount of radicals at a higher $LiNbO_3$ coating thickness is sufficient to degrade toluene at a high rate.

Percentage removals of toluene with respect to contact time of toluene with the surface of $LiNbO_3$-coated specimen are shown in Fig. 7. Percentage removal of toluene is found to be higher at the initial stage until 2 h, which is illustrated by an initial steeper slope curve. The initial higher toluene concentration causes the steeper slope. After approximately 2 h, the curves become flatter as toluene concentration decreases with time because of photodegradation. The same numbers of self-assembled system of $LiNbO_3$ on the surface are responsible for this degradation. The percentage removal of toluene for 0.25, 0.50, 0.75, and 1.00 mm coating thicknesses are found to be 53.3, 65.6, 79.5 and 79.2%, respectively after 6 h (Fig. 7), which are 22.6, 31.8, 47 and 48.3 %, respectively at 1 h. The small height of error bars in terms of standard deviation indicates the higher accuracy of collected data. The enhancement of removal rate is due to the increase in particle density in the illumination area. Percentage removals of ethyl benzene and toluene at different coating thicknesses after 6 h are summarized in Table-1, which indicates that the percentage removal of ethyl benzene at various

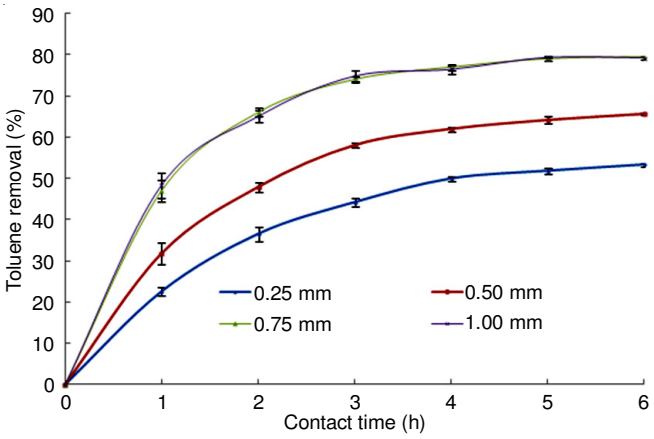

Fig. 7. Effect of depth of coating in percentage removal of toluene

TABLE-1
HIGHER REMOVAL PERCENTAGES OF EB AND TOLUENE AT DIFFERENT DEPTH OF COATING AFTER 6 h

Pollutant	Depth of coating (mm)	Percentage of removal after 6 h (%)
Ethyl benzene	0.25	58.97
	0.50	70.51
	0.75	82.42
	1.00	82.48
Toluene	0.25	52.49
	0.50	64.99
	0.75	79.50
	1.00	79.22

coating thicknesses is always higher than that of toluene. After 6 h, the percentage removals of ethyl benzene and toluene at 0.75 mm coating thickness containing concrete block are 82.42 and 79.5 %. The obvious factor related to this aspect is the structure of ethyl benzene and toluene. Both ethyl benzene and toluene are derivatives of benzene, which contains one methyl group. The ethyl group and methyl group in ethyl benzene and toluene seem to affect $LiNbO_3$ photoreactivity. Given the presence of steric hindrance in ethyl group, ethyl benzene is more reactive. Thus, photocatalytic oxidation using $LiNbO_3$ is very selective toward the structure of VOCs.

Effect of initial concentration of volatile organic compounds (VOCs): As a measure of air purification potential in this study, the removal efficiency of ethyl benzene and toluene from indoor air is investigated at different initial injected concentrations. To ensure data accuracy in ethyl benzene and toluene removal experiments, initial concentration is set at 50, 80 and 110 mg/L.

Removal of ethyl benzene: The removal rate of ethyl benzene under different initial concentrations with the contact time is shown in Fig. 8. Photocatalytic removal of ethyl benzene after 2.5 h shows a higher oxidation rate with a lower concentration than a higher concentration. This indicates the dependence of $LiNbO_3$ photoreactivities on ethyl benzene concentration. The reason for this is the collision within ethyl benzene molecules that decrease the activity of hydroxyl molecules as well as decrease the photocatalytic degradation rate. As the injected ethyl benzene concentration remains constant, the number of ethyl benzene molecules decreases while time increases. This finding explains why the degradation rate of higher initial ethyl benzene concentration (80 and 110 mg/L) is higher than that of lower initial concentration (50 mg/L) after 2.5 h. Relatively low height of error bar indicates that a steady state is maintained during sample collection.

Another possible reason is the amount of photocatalyst on the concrete surface and a high enough concentration of ethyl benzene in the photocatalytic reaction chamber so that catalyst surface is totally cluttered up with ethyl benzene. Increasing the concentration of ethyl benzene even more does not have any effect because the catalyst is already working at its maximum capacity.

Percentage removal of ethyl benzene degradation at different initial concentration are shown in Fig. 9. After 6 h, the percentage removal of ethyl benzene for initial concentration of 50, 80, and 110 mg/L are 82.42, 71.91 and 61.96 %, respectively. This result might be closely related to the attachment

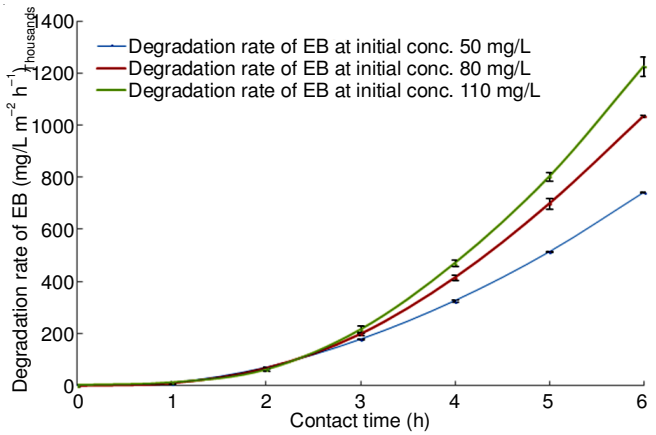

Fig. 8. Removal rate of EB at different initial concentration

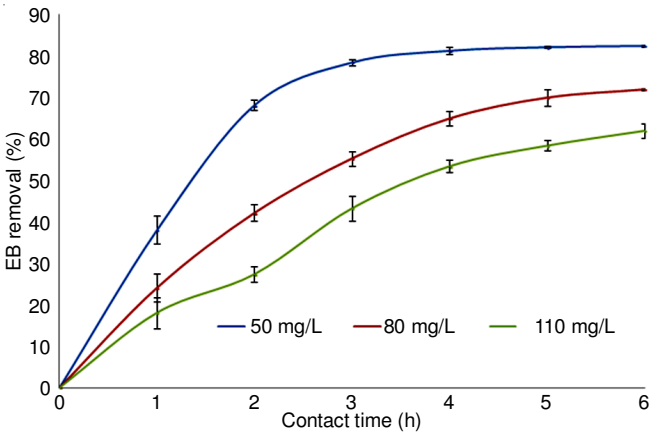

Fig. 9. Effect of initial concentration in the photo degradation of ethyl benzene

of ethyl benzene molecules onto the photocatalyst surface. It is higher than the study conducted by Hinojosa *et al.* [6], where only 59 % of ethyl benzene is removed at the same time at room temperature, although they used perlite granules coated with indium-doped TiO_2 to decompose ethyl benzene. With UV light irradiance, photocatalytic activity increased in relation to which light can penetrate to excite electron-hole pairs in catalyst coatings. Then, the reactant can accelerate to capture the electron or holes generated in catalyst surface and this leads to an increase in the speed of removal of pollutants [32].

The higher removal efficiency of $LiNbO_3$ in ethyl benzene degradation is due to the presence of $^{\bullet}OH$ radical on the catalyst surface. The $^{\bullet}OH$ radical generation is crucial in the photodegradation process because this substance oxidizes the organic VOCs to carbon dioxide and water. By increasing ethyl benzene concentration, more organic substances cover the active sites of $LiNbO_3$. If light intensity and irradiation time are constant, fewer photons would reach the catalyst surface, less $^{\bullet}OH$ radicals would be formed, and the relative number of $^{\bullet}OH$ radicals that attack the compound would also decrease. Thus, an inhibitory effect in photodegradation is anticipated.

Removal of toluene: Removal rate of toluene at different initial concentrations with contact time are shown in Fig. 10. Degradation rate of 50 mg/L initial concentration is higher until 2.5 h than at 80 and 110 mg/L. After 3 h, degradation rate of 110 mg/L initial toluene concentration is higher than others. This finding indicates that photocatalytic degradation of toluene depends on toluene concentration because of the collision among

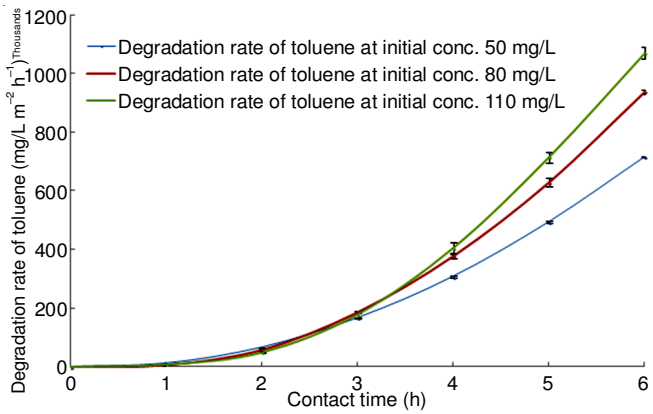

Fig. 10. Removal rate of toluene at different initial concentration

toluene molecules that decreases photocatalytic degradation rate.

Another possible cause for such results is the UV screening effect of toluene itself. A significant amount of UV may be absorbed at high toluene concentration by toluene molecules rather than $LiNbO_3$ particles, and that reduces the efficiency of the photocatalytic degradation reaction because of the decreased concentration in $^{\bullet}OH$ and O_2.

The percentage removal of toluene from indoor environment at different initial pollutant concentrations with contact time is shown in Fig. 11. The results showed that a decrease in VOC degradation is observed as the concentration increases. This finding might be closely related to VOC molecule attachment onto the photocatalyst surface. The percentage removal of toluene for initial concentration of 50, 80, and 110 mg/L are 79.5, 65.1 and 53.99 % respectively after 6 h. This result indicates that the rate of photocatalytic oxidation is dependent on the initial concentration of the pollutants. Lower initial concentration produces better photocatalytic oxidation rate of toluene removal. This observation is expected because the amount of toluene oxidized depends on the amount of radicals on the catalyst, which in turn depends on the number of holes generated on the catalyst. Therefore, at lower toluene concentration, the radicals generated by the holes are sufficiently high to degrade the low quantity of toluene. On the contrary, with higher toluene concentration, the amounts of the radicals are insufficient to degrade all toluene molecules.

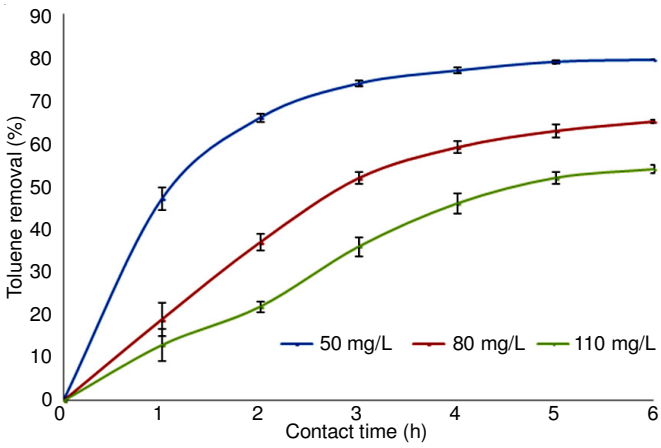

Fig. 11. Effect of initial concentration in removal of toluene

Comparison of percentage removal of ethyl benzene and toluene by $LiNbO_3$ and TiO_2

Ethyl benzene: The efficiency of $LiNbO_3$ photocatalyst in removing VOCs is determined by comparing the photodegradation of ethyl benzene in $LiNbO_3$ and TiO2-coated concrete. Fig. 12 shows the percentage removal efficiency of ethyl benzene in coating with $LiNbO_3$ and TiO_2 in concrete. About 82.42% ethyl benzene in $LiNbO_3$ and 73.25 % ethyl benzene in TiO_2 are removed within 6 h. This indicates that the percentage removal of ethyl benzene by $LiNbO_3$-coated concrete block is higher than that of TiO_2, regardless of contact time. The high-yield products in the case of $LiNbO_3$ over TiO_2 are due to its strong remnant polarization (70 μC/cm^2). $LiNbO_3$ obtained the highest percentage degradation of ethyl benzene among all of the other photocatalysts that are used in concrete construction. In addition, active considerations are suitable only for catalysts $LiNbO_3$ located close to the surface site at which the interfacial charge transfer occurs in the presence of UV light. UV light directly helps to increase the efficiency of $LiNbO_3$, leading to increased adsorption of pollutants because of its higher remnant polarization.

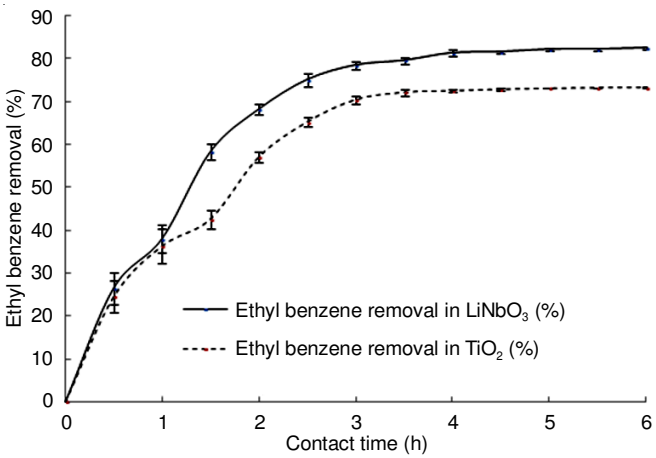

Fig. 12. Percentage removal of ethyl benzene in TiO_2 and $LiNbO_3$

Toluene: Percentage removal of toluene using $LiNbO_3$ and TiO_2-coated concrete surface are shown in Fig. 13. It shows that percentage removal of toluene in $LiNbO_3$ is higher than that of TiO_2 regardless of contact time. The small height of error bar in terms of standard deviation indicates that a steady state is maintained during sample collection. About 71.74 % toluene in TiO_2 and 79.53 % toluene in $LiNbO_3$ are degraded within 6 h. This finding is due to the charge separation of the generated carriers of photocatalyst which is higher in $LiNbO_3$ compared with that of TiO_2. The energy level conduction band of TiO_2 is lower than that of $LiNbO_3$. The charge transfer process can also be promoted, as more of the Nb^{3+} ions are distributed near the surface. Because of larger $LiNbO_3$ particle size than TiO_2, electron transfer become easier and improves the photocatalytic activity of $LiNbO_3$ because more ion radicals are formed.

Effect of ethyl benzene and toluene on microstructure of TiO_2 and $LiNbO_3$: The microstructures of the particles of TiO_2 and $LiNbO_3$ coated on the surface of concrete blocks are observed. Most of the scanning are made with 5-12 kX magnification and 10 kV scanning voltage. The thin layer of catalyst coated on the surface of concrete blocks is 0.75 mm thick and

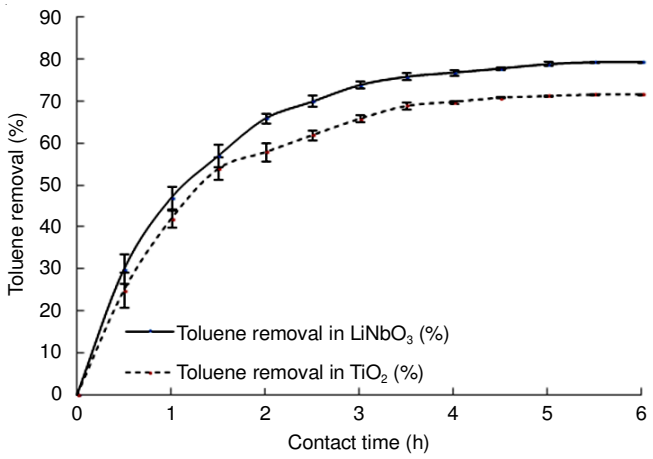

Fig. 13. Percentage removal of toluene in TiO_2 and $LiNbO_3$

uniformly covers the surface without originating cracks and segregation.

Fig.14 illustrated the SEM image of titanium dioxide before adsorption ethyl benzene on the concrete block surfaces. A dense structure with a uniformly distributed layer is observed in TiO_2. The morphology of the particles is spherical, brighter, and regular, with size ranging within 1.28-1.84 µm. However, the morphology of specimens after adsorption is converted in terms of shape, distribution of particles, and porosity. The SEM image of TiO_2 after adsorption pollutants on the sample surfaces is shown in Fig. 15, which shows that after the adsorption of pollutants onto the surface of concrete block. In this case, it is clear that a multi-layer of TiO_2 has no effect in degradation value. This could be explained that only the surface layer of the coating is fully in touch with pollutants and it only degrades the polluting substances.

The samples of concrete coated with $LiNbO_3$ before and after adsorption ethyl benzene are also observed by SEM as shown in Figs. 16 and 17. The morphology of the particles is spherical, brighter, and regularly with size ranging within 0.94-1.32 µm. These specimens show a more homogeneous surface, which has changed in terms of shape, particle distribution, and porosity. In addition, the morphology of sample surfaces and $LiNbO_3$ particles after adsorbed pollutants, the surfaces of the samples became very coarse. With larger magnification,

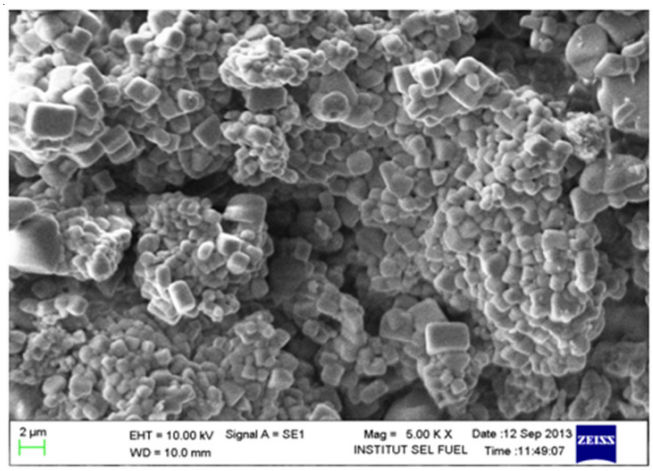

Fig. 14. SEM micrograph of TiO_2 thin layer before adsorption of ethyl benzene on concrete block surface

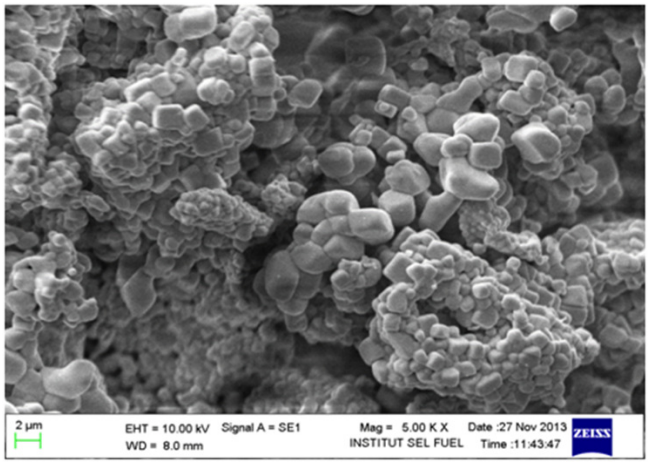

Fig. 15. SEM micrograph of TiO_2 thin layer after adsorption of ethyl benzene on concrete block surface

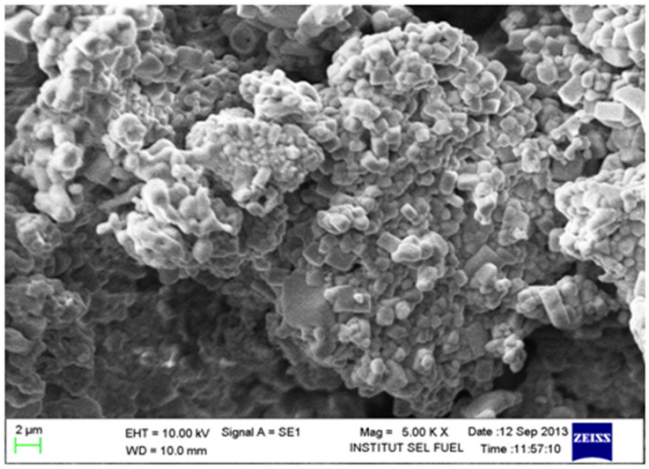

Fig. 16. SEM micrograph of $LiNbO_3$ thin layer before adsorption of ethyl benzene on concrete block surface

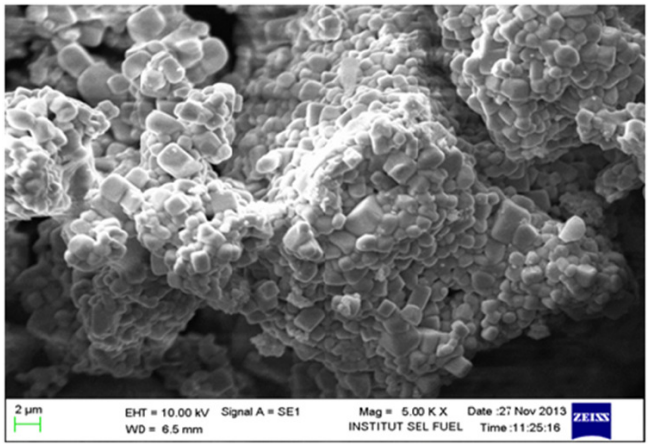

Fig. 17. SEM micrograph of $LiNbO_3$ thin layer after adsorption of ethyl benzene on concrete block surface

it is obvious that $LiNbO_3$ particles are nearly having a large reaction surface. Fig. 16 showed that $LiNbO_3$ has a large pore size and is homogeneously distributed before adsorption pollutants. Adsorption is observed to increase with increased pore size. The size of the pores is also related to the size of catalyst added. As the size of the catalyst particle becomes bigger, the pore size also increases. During the degradation reaction, these particles

would gradually increase along with the increase in adsorption pollutants, causing a decrease in the pore size [27]. The amount of pores formed on the surface of catalyst can be directly related to the porosity of thin layer. The more porous means the larger the surface area of the catalyst. This property is an advantage of thin layer as it provides a larger number of active sites for photocatalytic reactions to take place. Similar results have been reported by Yu *et al*. [33]. They investigated the influence of TiO_2 thin film in decreasing pollution.

A close look at Fig. 17 (micrograph of $LiNbO_3$ thin layer) revealed that agglomeration occurrs probably during adsorption and degradation. This agglomeration among particles of $LiNbO_3$ is more intense, which consequently increases with increased adsorption; thus, surface roughness is formed.

SEM images of $LiNbO_3$-coated concrete before and after adsorption of toluene is also observed. The morphology of $LiNbO_3$ coating types before and after applying toluene with a magnification of 12 kX is shown in Figs. 18 and 19. Similar results to those before and after ethyl benzene adsorption is observed in the SEM image of $LiNbO_3$ thin layer before and after toluene adsorption onto concrete block surface. This finding is due to the kind of pollutants absorbed onto the specimens' surfaces that do substantially affect the particle structures of catalyst on the samples. SEM results further confirmed that the reaction surface plays a curcial role in increasing pollutant removal efficiency. Moreover, $LiNbO_3$ shows higher particle agglomeration but good photoactivity for the degradation of target pollutants (ethyl benzene and toluene). Thus, $LiNbO_3$ shows higher reactive surface value and higher photodegradation ability of target pollutants than pure TiO_2.

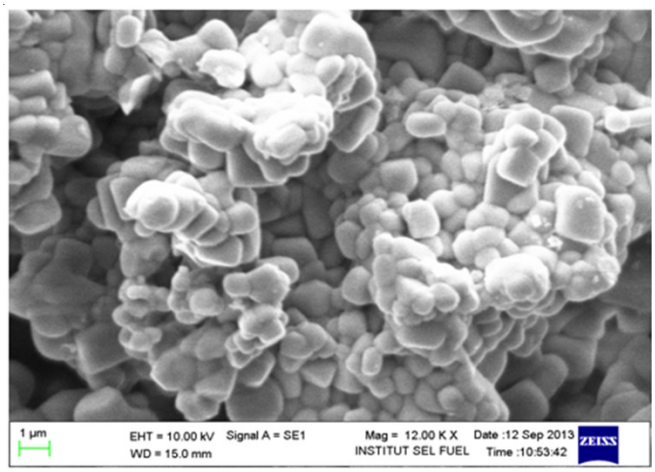

Fig. 18. SEM micrograph of $LiNbO_3$ thin layer before adsorption of toluene on concrete block surface

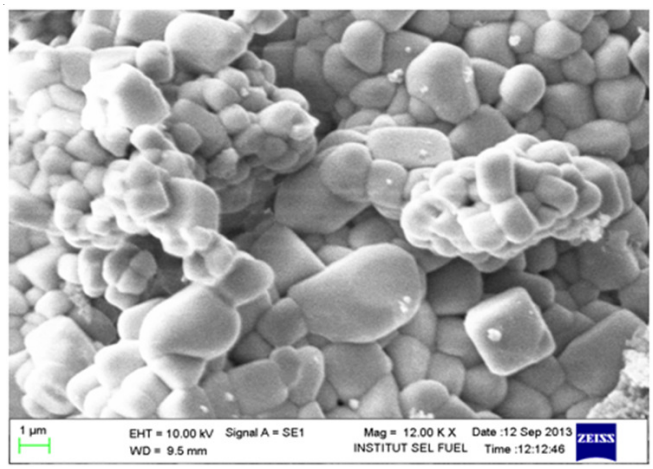

Fig. 19. SEM micrograph of $LiNbO_3$ thin layer after adsorption of toluene on concrete block surface

Conclusion

The development of innovative, sustainable technologies for environmental improvement is an absolute necessity. From the present study, the addition of $LiNbO_3$ to building materials is observed to confer some properties conducive to purifying indoor air. The thin layer of 0.75 mm of photocatalytic-coated concrete block is highly visible, active, and showed high photoreactivity. From indoor environment containing 50 mg/L pollutants, $LiNbO_3$-coated concrete can remove 82.42 % of ethyl benzene and 79.5 % of toluene within 6 h in the presence of light. In this sense, $LiNbO_3$-coated photocatalytic cements contribute significantly, which can be widely implemented in the construction industries.

REFERENCES

1. J. Zhao and X. Yang, *Build. Environ.*, **38**, 645 (2003); https://doi.org/10.1016/S0360-1323(02)00212-3.
2. M. Hunger, G. Husken and H.J.H. Brouwers, *Cement Concr. Res.*, **40**, 313 (2010); https://doi.org/10.1016/j.cemconres.2009.09.013.
3. F. Benoit-Marquié, U. Wilkenhöner, V. Simon, A.M. Braun, E. Oliveros and M.-T. Maurette, *J. Photochem. Photobiol. Chem.*, **132**, 225 (2000); https://doi.org/10.1016/S1010-6030(00)00196-9.
4. P. Blondeau, V. Iordache, O. Poupard, D. Genin and F. Allard, *Indoor Air*, **15**, 2 (2005); https://doi.org/10.1111/j.1600-0668.2004.00263.x.
5. B.E. Butterworth, *Regul. Toxicol. Pharmacol.*, **45**, 9 (2006); https://doi.org/10.1016/j.yrtph.2006.01.011.
6. R.M. Hinojosa, S. Arriaga, T.L.A. Diaz and G.V. Rodríguez, *Chem. Eng. J.*, **224**, 106 (2013).
7. D. Norback, E. Bjornsson, C. Janson, J. Widstrom and G. Boman, *Occup. Environ. Med.*, **52**, 388 (1995); https://doi.org/10.1136/oem.52.6.388.
8. L.-A. Galeano, M.Á. Vicente and A. Gil, *Catal. Rev., Sci. Eng.*, **56**, 239 (2014); https://doi.org/10.1080/01614940.2014.904182.
9. B. Zielinska and A.W. Morawski, *Appl. Catal. B*, **55**, 221 (2005); https://doi.org/10.1016/j.apcatb.2004.08.015.
10. A.P. Jones, *Atmos. Environ.*, **33**, 4535 (1999); https://doi.org/10.1016/S1352-2310(99)00272-1.
11. M. Stock and S. Dunn, *IEEE Trans. Ultrason. Ferroelectr. Freq. Control*, **58**, 1988 (2011); https://doi.org/10.1109/TUFFC.2011.2042.
12. G. Clausen, O. Alm and P.O. Fanger, 9th International Conference on Indoor Air Quality and Climate, June 30 - July 5 Monterey, California, vol. 1, p. 338 (2002).
13. R.K. Nath, M.F.M. Zain, A.A.H. Kadhum and A.B.M.A. Kaish, *Constr. Build. Mater.*, **54**, 348 (2014); https://doi.org/10.1016/j.conbuildmat.2013.12.072.
14. M. Hinojosa-Reyes, V. Rodríguez-González and S. Arriaga, *J. Hazard. Mater.*, **209-210**, 365 (2012); https://doi.org/10.1016/j.jhazmat.2012.01.035.
15. H.K. Dong, H.C. Dong, S.Y. Myoung and W.K. Kwang, *J. Adhes. Sci. Technol.*, **27**, 5 (2013).
16. G.L. Guerrini, *Constr. Build. Mater.*, **27**, 165 (2012); https://doi.org/10.1016/j.conbuildmat.2011.07.065.
17. M. Safari, M. Rostami, M. Alizadeh, A. Alizadehbirjandi, S.A. Nakhli and R. Aminzadeh, *Iran. J. Environ. Health Sci. Eng.*, **12**, 1 (2014); https://doi.org/10.1186/2052-336X-12-1.
18. C. Akly, P.A. Chadik and D.W. Mazyck, *Appl. Catal. B*, **99**, 329 (2010); https://doi.org/10.1016/j.apcatb.2010.07.002.

19. Y. Jiang, P. Zhang, Z. Liu and F. Xu, *Mater. Chem. Phys.*, **99**, 498 (2006); https://doi.org/10.1016/j.matchemphys.2005.11.036.
20. K.P. Kuhn, I.F. Chaberny, K. Massholder, M. Stickler, V.W. Benz, H.-G. Sonntag and L. Erdinger, *Chemosphere*, **53**, 71 (2003); https://doi.org/10.1016/S0045-6535(03)00362-X.
21. R.K. Nath, M.F.M. Zain and A.A.H. Kadhum, *Sci. World J.*, **Article ID 686497** (2013). https://doi.org/10.1155/2013/686497.
22. L. Laokiat, P. Khemthong, N. Grisdanurak, P. Sreearunothai, W. Klysubun and W. Pattanasiriwisawa, *Korean J. Chem. Eng.*, **29**, 377 (2012); https://doi.org/10.1007/s11814-011-0179-1.
23. H. Chen, A. Namdeo and M. Bell, *Environ. Model. Softw.*, **23**, 282 (2008); https://doi.org/10.1016/j.envsoft.2007.04.006.
24. A. Folli, U.H. Jakobsen, G.L. Guerrini, D.E. Macphee and B. Rhodamine, *J. Adv. Oxid. Technol.*, **12**, 126 (2009); https://doi.org/10.1515/jaots-2009-0116.
25. L. Zou, Y. Luo, M. Hooper and E. Hu, *Chem. Eng. Process.*, **45**, 959 (2006); https://doi.org/10.1016/j.cep.2006.01.014.
26. Q.L. Yu and H.J.H. Brouwers, *Appl. Catal. B*, **92**, 454 (2009); https://doi.org/10.1016/j.apcatb.2009.09.004.
27. A. Fujishima, T.N. Rao and D.A. Tryk, *J. Photochem. Photobiol. Photochem. Rev.*, **1**, 1 (2000); https://doi.org/10.1016/S1389-5567(00)00002-2.
28. G. Husken, M. Hunger, H. Brouwers, P. Baglioni and L. Cassar, *Build. Environ.*, **44**, 2463 (2009); https://doi.org/10.1016/j.buildenv.2009.04.010.
29. A.Z. Simoes, A.H.M. Gonza'lez, A.A. Cavalheiro, M.A. Zaghete, B.D. Stojanovic and J.A. Varela, *Ceram. Int.*, **28**, 265 (2002); https://doi.org/10.1016/S0272-8842(01)00089-X.
30. W.C. Yang, B.J. Rodriguez, A. Gruverman and R.J. Nemanich, *Appl. Phys. Lett.*, **85**, 2316 (2004); https://doi.org/10.1063/1.1790604.
31. M. Stock and S. Dunn, *Ferroelectrics*, **419**, 9 (2011); https://doi.org/10.1080/00150193.2011.594399.
32. A. Fujishima, X.T. Zhang and D.A. Tryk, *Surf. Sci. Rep.*, **63**, 515 (2008); https://doi.org/10.1016/j.surfrep.2008.10.001.
33. C.J. Yu, J. Yu, W. Ho and J. Zhao, *J. Photochem. Photobiol. Chem.*, **148**, 331 (2002); https://doi.org/10.1016/S1010-6030(02)00060-6.